Available online at www.sciencedirect.com
SCIENCE DIRECT®
Journal of Sound and Vibration 279 (2005) 1097–1120
JOURNAL OF SOUND AND VIBRATION
www.elsevier.com/locate/jsvi

Particle damping for passive vibration suppression: numerical modelling and experimental investigation

Zhiwei Xu[a], Michael Yu Wang[b,*], Tianning Chen[c]

[a] *The Aeronautical Science Key Laboratory for Smart Materials and Structures, Nanjing University of Aeronautics and Astronautics, Nanjing, China*

[b] *Department of Automation and Computer-Aided Engineering, The Chinese University of Hong Kong, Shatin, NT, Hong Kong, China*

[c] *College of Mechanical Engineering, Xi'an Jiaotong University, Xi'an, China*

Received 19 November 2002; accepted 28 November 2003

Abstract

As a simple and passive means, particle damping provides vibration suppression with granular particles embedded within their containing holes in a vibrating structure. Unlike in traditional damping materials, mechanisms of energy dissipation of particle damping are primarily related to friction and impact phenomena which are highly non-linear. In the research work reported in the paper we investigate elastic beam and plate structures with drilled longitudinal holes filled with damping particles. Our focus is on the form of damping due to shear friction induced by strain gradient along the length of the structure. We present physical models to take into account of the shear frictional forces between particle layers and impacts of the particles with the containing holes. A numerical procedure is presented to predict the damping effect. Experimental tests of the beam and plate structures for various different damping treatments are also conducted. Model predictions are validated by experimental results.

The particle damping is found to be remarkably strong for a broadband range. Moreover, the shear friction is determined to be the major contributing mechanism of damping, especially at a high volumetric packing ratio. The numerical and experimental findings suggest that the best damping effect might be achieved by using a design of multiple particle chambers involving an appropriate combination of the impact, friction and shear mechanisms, in contrast to a transverse-type particle or single-mass damper.

*Corresponding author. Tel.: +852-2609-8487; fax: +852-2603-6002.
E-mail address: yuwang@acae.cuhk.edu.hk (M.Y. Wang).

0022-460X/$ - see front matter
doi:10.1016/j.jsv.2003.11.023

1. Introduction

Particle damping is a passive damping concept to use metal or ceramic particles or powders of small size (~0.05–5 mm in diameter) that are placed inside cavities within or attached to the vibrating structure as illustrated schematically in Fig. 1. Metal particles of high density such as lead or tungsten steel (as shown in Fig. 2) are the most common materials for better damping performance. In contrast to viscoelastic materials which dissipate the stored elastic energy [1], particle damping treatment focuses on energy dissipation in a combination of collision, friction and shear damping [2,3]. It involves the potential of energy absorption and dissipation through momentum exchange between moving particles and vibrating walls, friction, impact restitution, and shear deformations. It is an attractive alternative in passive damping due to its conceptual simplicity, potential effectiveness over broad frequency range, temperature and degradation insensitivity, and very low cost [2–9].

Particle damping is a derivative of single-mass impact damper that has been thoroughly studied over the years (e.g., Refs. [10,11]). In the single-mass case, direct analyses exist and reveal design criterion for optimal efficiency based on reduction in system response. It is observed through experiments that a plastic "bean bag" filled with lead shot exhibited much greater damping effectiveness and "softer" impacts than a single lead slug of equal mass [12,13]. Additional benefits of using granular materials instead of a single mass include the elimination of excessive noise and potential damage to the interior wall of the containing hole. Although the initial test results of the early 1990s substantiated the potential of particle damping [2–5], applications in the literature have been largely based only on heuristic guidelines [3]. Due to the complex interactions involved in particle damping, a comprehensive modelling and analysis tool is yet available [6–9]. This technology has been considered as a speciality area and the literature is relatively scarce. The list of references of the paper represents an extensive but not exhaustive effort of literature survey of the speciality technology.

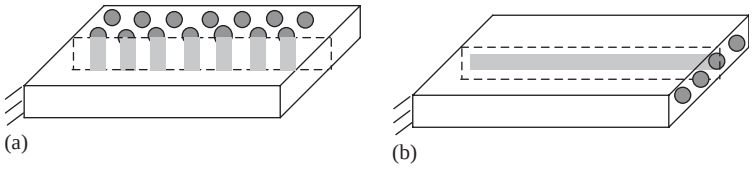

Fig. 1. Schematic of a beam with (a) transverse particle dampers or (b) longitudinal particle dampers.

Fig. 2. Metal particles as damping material: lead particles (left) and tungsten carbide particles (right).

There have been some research efforts toward analytical or numerical models of the complicated phenomenon of multi-grain particle damping [6,8]. Most noticeable efforts have recently been given to the discrete element method (DEM) with some limited studies of particle dampers [8,14–16]. This is a technique originally developed for the simulation of behavior of granular materials [17,18]. Over the years, the DEM has found a wide range of applications in various disciplines (see Refs. [19,20]). The procedure is an explicit process with small time step iterations to determine resultant forces on any particle in the system. Because of the very large number of particles in a typical particle damper, it appears that the concept of the damping modelling on a particle-to-particle basis is a computationally intensive task [15,16], although it offers the potential for a deeper understanding of the particle damping mechanisms.

In this paper, we study an elastic beam and a plate treated with particle damping for suppression of vibrations. Fig. 1 shows the beam of a constant rectangular cross-section with holes drilled along its length. Metal particles are filled within these longitudinal holes. We present a numerical model for the analysis and characterization of the particle damping effect. In particular, the model captures the dominant mechanisms of particle damping, including energy dissipation by impact and friction during inter-particle and particle–wall collisions and by shear action due to strain gradient in the longitudinally packed particles. This modelling capability allows us to characterize the non-linear properties of particle damping and the relative effectiveness of these damping mechanisms in terms of a host of parameters such as particle size, packing density, and frequency and amplitude of excitation. Under different parameters of the system, impact, friction and shear action may play a different role in providing a significant portion of energy dissipation for vibration attenuation. The modelling technique is believed to be important, since it would facilitate the development of design methods for achieving high damping effect from the use of a minimal quantity of particles.

In this article we focus on the development of physical models for the different damping mechanisms and of a numerical analysis of the vibration of the damped beam and plate structures under forced excitation. Numerical results of the analysis will be presented. The results will be compared with a set of experimental measurements of a beam and a plate with the particle damping treatment. Thus, the modelling and analysis technique described in this paper is experimentally validated.

2. The beam with particle damping treatment

In particle damping treatment of a beam, many containing holes (or cavities) may be used to distribute particle material over the structure. There are two common arrangements in terms of the orientation of the holes with respect to the direction of vibration motion: transversal and longitudinal, as shown in Fig. 1. The transversal type is typical and has been studied in nearly all the literature on particle damping [2–9]. One reason might be that the strain gradient along a transversal hole could be neglected, thus simplifying the damping behavior of the particles. On the other hand, the strain gradient along the longitudinal hole could cause a significant shear stress in packed particles. While this phenomenon offers another mechanism for energy dissipation, it increases the level of complexity in modelling and analysis of damping effects. We make a particular effort in this study to include the shear action in order to make an assessment of its

significance. The beam is chosen for this study, in part, because it is an infinite d.o.f. system as opposed to the single d.o.f. systems usually studied in the literature [6–8,15,16]. When excited by a shaker, the beam response could exhibit a large number of modes. This would allow us to investigate the broadband effect of particle damping.

3. Particle characteristics

The application of particles is relatively simple. Metal or ceramic particles or powders of small size are directly placed inside the containing holes with the holes partially or wholly filled. The size of the particles is typically less than $\frac{1}{5}$ of the hole size in diameter and is usually in the range 0.05–1 mm in diameter. Thus, it is not uncommon that a single hole may contain a large number of particles in an order of 1000 or even 10 000. Metal particles of high density such as lead or tungsten carbide cobalt are usually the best choice (Fig. 2). Within this size range, the particles are considered non-cohesive.

3.1. Particle size

The photographs in Fig. 2 show that the lead particles are spheroidal while the shapes of tungsten particles are quite irregular. In our numerical model, the particles are assumed to be spherical and uniform in diameter. The sphere diameter ϕ is defined with an average of the measured minimal diameter of particles used. A number of past investigations have shown that the shape of particles is not a significant factor once the particle size is less than $\frac{1}{5}$ of the hole size [8,9].

3.2. Internal physical parameters

For granular particles contained in a cavity, there exist two important parameters characterizing the relationships of the internal stresses of the particle assembly. The first is the *internal coefficient of friction* μ [21]. Unlike its counterpart for the contact between two large bodies, the internal friction coefficient of a particle assembly is typically higher and is measured using a standard testing procedure to evaluate the shear force in the interface of two layers of the particles [21]. In a similar fashion, the friction between the particles and the surface of their containing wall is defined by another internal coefficient of friction μ_w. These internal friction coefficients depend on the types of materials as well as on the particle size. Table 1 lists the internal friction coefficients for particles of an average diameter $\phi = 0.1$ mm for three different

Table 1
Internal friction coefficient of particles ($\phi = 0.1$ mm)

	Material		
	Aluminum	Stainless steel	Tungsten carbide
μ	0.21	0.27	0.35

Table 2
Internal friction coefficient of particles of different sizes

	ϕ (mm)		
	0.1	0.3	0.5
Tungsten carbide	0.35	0.40	0.47
Stainless steel	0.27	0.31	0.36

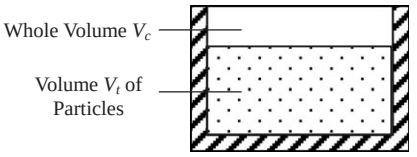

Fig. 3. A schematic of particles filled in a volume.

materials, respectively [21], while in Table 2 the coefficients are shown to change when the particle size changes.

Another important parameter is the pressure correlation coefficient K_a [21]. Essentially, it defines the ratio of the normal stress in the horizontal direction to that in the vertical direction when the particle assembly is subject to either a horizontal or a vertical pressure [21].

3.3. Packing of particles

Each containing hole may be filled with particles fully or partially. As shown in Fig. 3, a containing hole has a total volume of V_c and its portion occupied by the filled particles is denoted by V_t. Thus, we define the volumetric packing ratio Θ as

$$\Theta = V_t/V_c. \tag{1}$$

It should be noted that within the filled volume V_t of the containing hole there are unoccupied cavity spaces between the particles. This may be measured by the *particle filling ratio* ψ defined as

$$\psi = m/\rho V_t \tag{2}$$

for a total mass m of the filled particles of mass density ρ. For spherical particles of radius r, we may assume that the particles are packed in layers inside the containing hole. Then, it is easy to find that the particle filling ratio has a minimum of $\psi_{min} = 52.36\%$ and a maximum of $\psi_{max} = 74.06\%$, respectively, corresponding to the particle arrangements shown in Fig. 4 [21]. At the minimum filling, the distance between two adjacent particle layers is at maximum, $s_{max} = 2r$, while at the maximum filling this distance is reduced to $s_{min} = (2\sqrt{6}/3)r \approx 1.633r$.

In practical situations the particles do not arrange themselves in perfect layers and, in fact, they should be considered to be packed randomly. During the course of a vibration, they tend to get more packed from their initial packing state. This is a well-known fact [21]. In our experience of packing the tungsten carbide particles ranging between $\phi = 0.1$ and 0.5 mm within a hole of 6 mm in diameter, the particle filling ratio reaches a maximum of approximately $\psi = 62.5\%$ when particles are repeatedly filled in the hole after a series of shaking motions until the

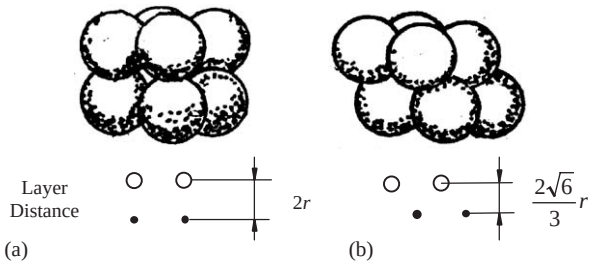

Fig. 4. Particle layers of theoretical separation. (a) Minimum distance and (b) maximum distance.

volumetric packing ratio remains near 100%. Our finding is consistent with previous experimental results [21].

Therefore, after some initial shaking and vibration, the particles could be considered being packed with an approximate filling ratio of $\psi = 62.5\%$. If the particles were distributed in layers, the distance between two adjacent layers s would be between the theoretical minimum and maximum, $1.633r = s_{min} < s < s_{max} = 2r$. The layer distance may be estimated with a linear interpolation between these two theoretical limits such as

$$\frac{\psi_{max} - \psi_{min}}{s_{min} - s_{max}} = \frac{\psi_{max} - \psi}{s_{min} - s}. \tag{3}$$

Thus, we have

$$s = (2.886 - 1.691\psi)r \tag{4}$$

and at the practical filling limit of $\psi = 62.5\%$, the layer distance is estimated to be

$$s = 1.83r. \tag{5}$$

This relation allows us to estimate a total number M of layers of particles for a given particle size, hole geometry and its volumetric packing ratio Θ.

4. Energy dissipation by frictional shear

In this section we describe a model for the energy dissipation due to shear forces between layers of the particles. Within each longitudinal hole, the bending motion of the beam will induce strain gradient along the length of the beam. Therefore, there exists a relative slip motion between adjacent layers of particles. Given the frictional nature of granular materials, the internal slip motion will cause frictional energy dissipation between the layers. This form of energy dissipation provides another damping mechanism in additional to kinetic energy dissipation due to particle impacts.

4.1. Transversal pressure

In order to evaluate the shearing friction forces, we first need to determine the transversal pressure between the particle layers. Its analysis is based on a standard procedure of powder mechanics [21]. Fig. 5 shows a longitudinal hole of radius R filled with particles of mass density ρ.

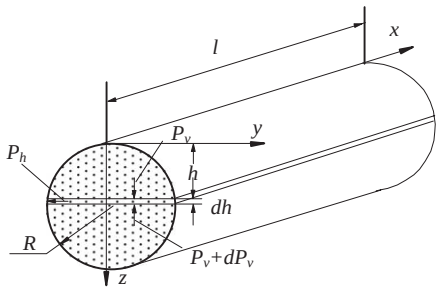

Fig. 5. Vertical pressure in the particles.

Along the transversal direction in z-axis, suppose the vertical pressure at vertical depth h to be P_v. It is well established in powder and soil mechanics that the normal pressure is described by the following differential form [21]:

$$\mathrm{d}h = \frac{\sqrt{h(2R-h)}}{\rho\sqrt{h(2R-h)} - K_a P_v \mu_w}\,\mathrm{d}P_v, \tag{6}$$

where K_a is the pressure correlation coefficient and μ_w is the internal friction coefficient between the particles and the containing hole as defined in Section 3.2. Thus, it is easy to find a formula for the normal pressure once we know the boundary condition at the top layer of the particles at $h = h_0$. For example, for a fully packed hole of $\Theta = 1.0$, we know that $P_v = 0$ at $h_0 = 0$. Then, we obtain

$$P_v = \frac{\sqrt{h(2R-h)}}{K_a\mu_w}\left[\rho - \exp\left(-\frac{h}{\sqrt{h(2R-h)}}K_a\mu_w\right)\right]. \tag{7}$$

It is interesting to note that the normal pressure P_v along the transversal direction is highly non-linear, depending on the particle mass density and the friction coefficient for the particle–wall interface. In Fig. 6, the pressure is plotted along the transversal depth h for three cases of different ρ. It shows that the pressure increases steadily from the top towards the bottom of the hole. However, near the very bottom ($h = 2R$), the normal pressure decreases rapidly and then vanishes at the bottom surface. This phenomenon is related to a unique property of granular materials that the internal friction between the particle–particle interface and the particle–wall interface forms a local energy state of the particle arrangements far from the globally minimal energy state [19–22]. Figs. 6 and 7 show how the vertical pressure changes with respect to different values in the particle mass density and the internal coefficient of friction of the particle–wall interface.

4.2. Shear energy

Given the transversal pressure between layers of particles, we may model the energy dissipation by the frictional shear as follows. For simplicity, we treat the particles in their layer formation during the bending motion of the beam, with a total of M layers. For two adjacent particle layers $(i-1)$ and (i) as shown in Fig. 8 ($i = 1, \ldots, M$), the shear strain of the beam at the interface

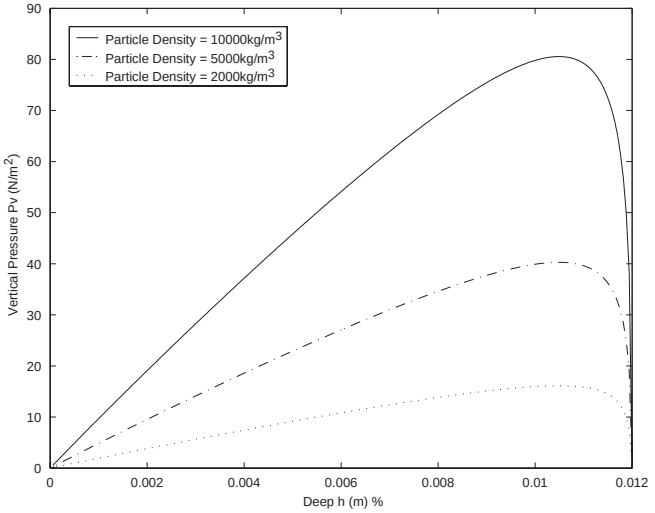

Fig. 6. Vertical pressure along the depth of the hole for three different particle densities, with $K_a = 0.7, \mu_w = 0.3$, and $R = 6$ mm.

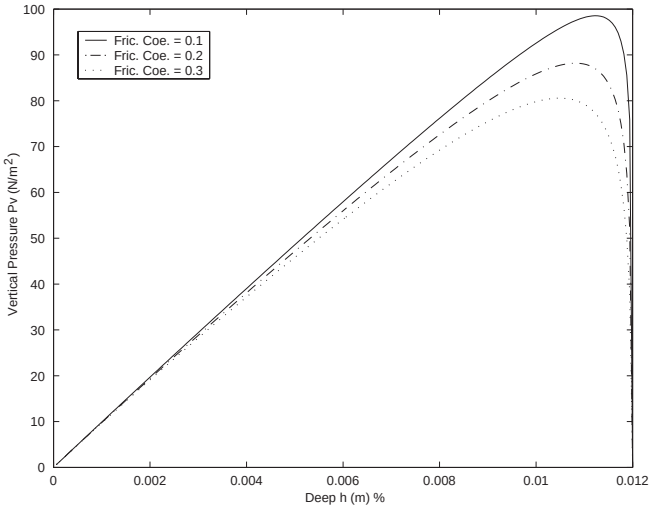

Fig. 7. Vertical pressure along the depth of the hole for three different friction coefficient values of μ_w, with $K_a = 0.7$, $\rho = 10\,000$ kg/m^3, and $R = 6$ mm.

position y_i between the layers is denoted by $\varepsilon_s(x, y_i)$. At this position y_i, the interface plane of the two layers has a width $b(y_i)$. Therefore, energy dissipation due to the interfacial friction between these two layers is described by

$$E_i = \int_0^L \varepsilon_s(x, y_i)\mu P_v(y_i)b(y_i)\,\mathrm{d}x, \tag{8}$$

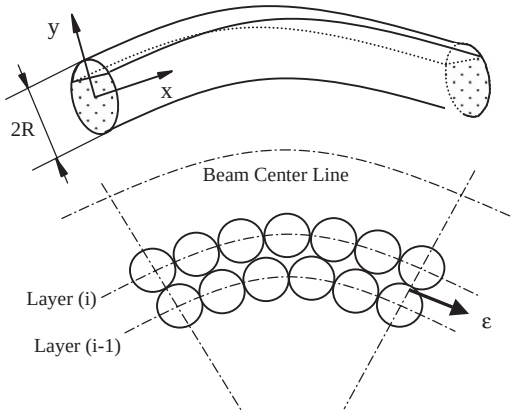

Fig. 8. Shear strain between layers of particles.

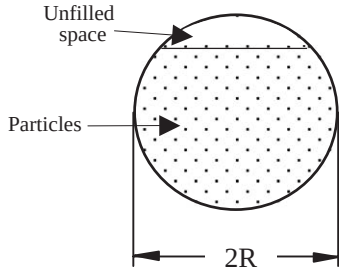

Fig. 9. Unfilled space inside a longitudinal hole.

where L is the length of the beam and P_v is described by Eq. (6). Summing over all layers of particles, the shear energy dissipation of the particles is given as

$$E_s = \sum_{i=1}^{M} \int_0^L \varepsilon_s(x, y_i)\mu P_v(y_i) b(y_i)\,\mathrm{d}x. \tag{9}$$

5. Particle impacts

During the vibration of the beam, the particles may impact with the surface of the containing hole if there exists any gap (i.e., when $\Theta < 100\%$) as shown in Fig. 9. Furthermore, the particles may collide with each other. Each collision will result in kinetic energy dissipation since the particles are not perfectly elastic. This form of "kinetic damping" has been regarded as a unique feature of particle damping, when using either a single mass or granular materials [2–16].

The particle–particle and particle–wall collisions bring a considerably high level of complexity for their modelling and damping analysis, especially for particle dampers of transversal holes lightly filled with small-size particles [6–9]. When the motions of particles are modelled as

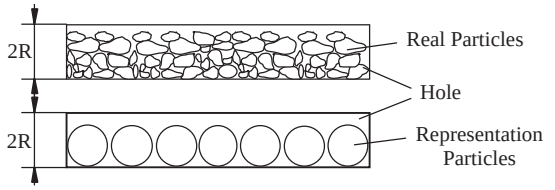

Fig. 10. Representation of particles for impact modelling.

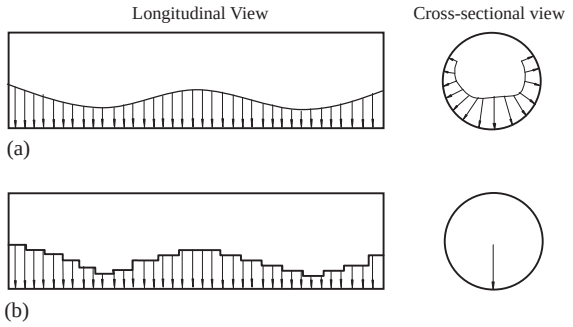

Fig. 11. Impacting force on the cavity wall. (a) Realistic distribution of impacting forces, and (b) impact force representation in the model.

a two-phase dense flow or on a particle–particle basis, the computational complexity is bound to be overwhelming [14–18]. We seek a more appropriate model in this study.

In our beam–damper system the particles are packed in a longitudinal hole. The open space unoccupied by the particle material is relatively small, especially for a high volumetric packing ratio Θ. The effect of impact of the particles with the containing hole is approximated by a simplified representation of a single row of spheres of a larger diameter as illustrated in Fig. 10. The total mass of these representative spheres would be equal to the sum of the masses of the original particles. Furthermore, only the impacts of these spheres with the wall of the hole are considered. The spheres are assumed to vibrate in the transversal direction only. Thus, interactions between the spheres are not represented. This is a simplification that has been employed previously in Ref. [23]. It was experimentally validated to be acceptable with a reasonable level of accuracy.

With this model of impacting spheres, we can readily apply a collision model to determine energy dissipation during a sphere–wall impact. Such a model has been a key element in the research works on multi-body dynamics [24] and granular materials [25] reported in a vast literature. We adapt the classical Hertz model considering the material parameters of Young's modulus and Poisson's ratio, as reported in our earlier works [15,16]. Since the model is rather standard, we leave out its details here.

Inside the longitudinal hole of the beam, the vibrating particles would practically generate impact forces normal to the surface of the hole and distributed over the entire area of contact between the particles and the hole. This is schematically shown in Fig. 11. Our model of impacting spheres would approximate only the net effect of the distributed forces as vertical forces and distributed only on the bottom line of the cylindrical hole. The distribution of the impacting forces would be predicted in relation to the motion of the beam.

6. Numerical calculation of beam response

With the models of shear friction and particle impacts described above, we are ready to develop a numerical procedure for calculating the response of the beam treated with the particle dampers for its free vibration or forced response. This would allow us to predict the effects of particle dampers and to conduct parametric studies of their performance.

6.1. The beam equation

For our numerical and experimental investigations, we use a free–free beam of a constant cross-section with longitudinal particle holes as depicted in Fig. 12.

If the longitudinal holes drilled in the beam have little effect on the principal modal motions of the beam (as experimentally verified and described in Section 7), the treated beam can be described as a Bernoulli–Euler beam. We may use a loss factor η to describe the internal damping in the beam, including the shear energy loss due to frictional shear action of the particles as modelled in Section 4. The loss factor depends on the longitudinal position, i.e., $\eta = \eta(x, t)$. The loss factor can be incorporated in the complex elastic modulus $E(1 + i\eta)$ of the beam. In addition to the frictional shear damping, the particle impacting forces as modelled in Section 5 are explicitly defined acting on the beam such that

$$F(x,t) = \sum_{j=1}^{n} f_{(j,t)}\delta(x - a_j), \tag{10}$$

where a_j indicates the position of the contact force of jth impacting sphere along the length of the beam for a total of n spheres as described in Section 5. Thus, the dynamic response of the beam is described by the following standard beam equation:

$$\frac{\partial^2}{\partial x^2}\left(E(1 + i\eta)J\frac{\partial^2 y}{\partial x^2}\right) + \rho_b A\frac{\partial^2 y}{\partial t^2} = F + G, \tag{11}$$

where ρ_b is the mass density of the beam, A is the cross-sectional area, J is the moment of inertia of the cross-section, and G is the point excitation force. The beam response $y(x, t)$ can be solved in terms of the principal modes of the beam in a numerical iteration process to be described below. As a standard procedure, for example, the initial conditions of the beam are given as

$$y(x,0) = f_1(x), \quad \left.\frac{\partial y}{\partial t}\right|_{t=0} = f_2(x). \tag{12}$$

Between a small time interval Δt of numerical simulation, we may use a constant value for η and for an impacting force. For brevity, we use the case of a single impacting force acting at a as an

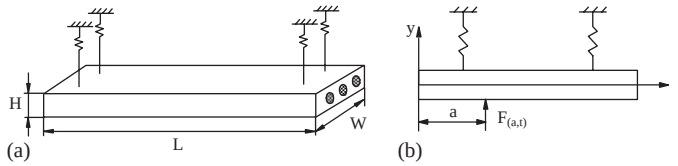

Fig. 12. A sketch of the test beam (a) with a point force applied (b).

example. Then,

$$F(a) = f_{(a)}\delta(x-a) \tag{13}$$

and the forced response is expressed by

$$Y(x,t) = \sum_{k=1}^{\infty}\left\{ Y_{k(x)} \exp\left(-\frac{\eta}{2}\omega_k t\right)\left[C_k \cos(\omega_k t) + D_k \sin(\omega_k t) + \frac{1}{(1+\eta^2/4)\omega_k^2} f_a Y_{k(a)}\left(\exp\left(\frac{\eta}{2}\omega_k t\right) - \cos[\omega_k t] - \frac{\eta}{2}\sin[\omega_k t]\right)\right]\right\}, \tag{14}$$

where

$$C_k = \int_0^l \rho_b A f_1(x) Y_k(x)\,\mathrm{d}x, \quad D_k = \frac{1}{\omega_k}\int_0^l \rho_b A f_2(x) Y_k(x)\,\mathrm{d}x + \frac{\eta}{2}a_k \tag{15}$$

and ω_k is the kth natural frequency and Y_k represents the kth modal shape of the beam [26]. However, the beam response is coupled with the loss factor of the internal damping and the energy dissipation of particle–hole impacts. The non-linear nature of the particle damping requires an iterative procedure to obtain the beam response over a given period of time.

6.2. Iterative procedure of simulation

The iterative procedure for numerical calculation of beam motion as well as the shear and impact damping is similar to a technique used in the DEM often found in the literature of granular materials and particle technology [16–20]. The motions of the beam and the particle are calculated through a cycling process of small time steps Δt. As the beam vibrates causing the shear strain and oscillations in the particles, the shear frictional forces would increase between the particle layers and the particles may collide with the containing wall as well (as predicted by using their representing spheres). These phenomena will dissipate energy from the beam, thus providing a combined damping effect that will act on the beam in turn. Thus, in the end of each time step Δt, the internal loss factor as well as the impacting forces is updated as a result of the beam motion. The cycle of beam and particle motion calculation is repeated for the next time step. The iterative procedure is summarized in the flow chart of Fig. 13. This incremental updating scheme was fully described in Ref. [17] and it has been widely tested in the literature [18–20], showing that it is reasonably accurate and stable when the time step Δt is properly chosen. In our numerical investigation, we found that it is satisfactory to use $\Delta t = 2.0 \times 10^{-5}$ s.

7. Experimental investigation

We have conducted an experimental investigation of the damped beam system to verify our numerical model and to make an assessment of the performance of the particle damping. A steel beam specimen is sketched in Fig. 12 with dimensions of $L = 500$ mm, $W = 50$ mm, and $H = 15$ mm. The steel beam is specified with a mass density of 7800 kg/m^3, an elastic modulus of 2×10^{11} N/m^2, and Poisson ratio of 0.3. The beam mass is 2.925 kg. Three longitudinal holes of

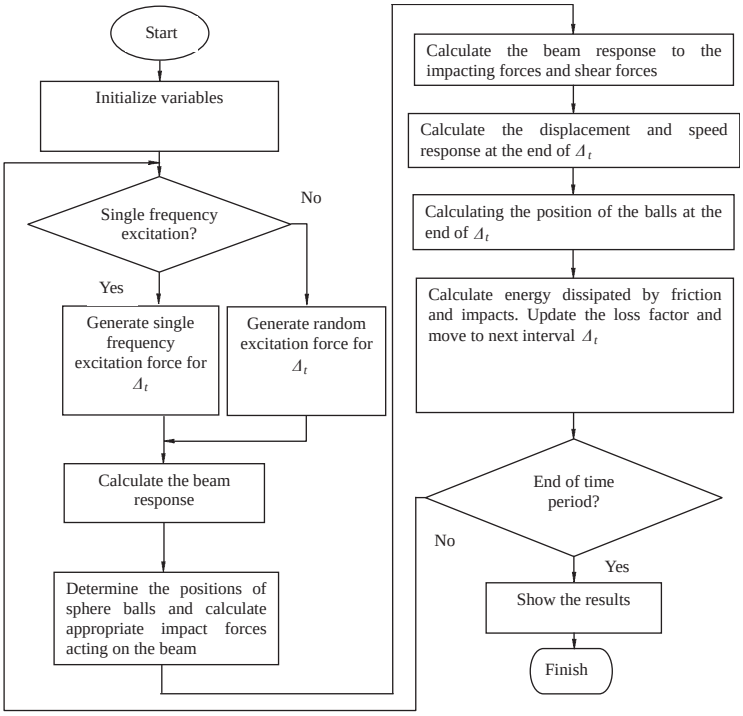

Fig. 13. Flow chart of the iterative numerical procedure.

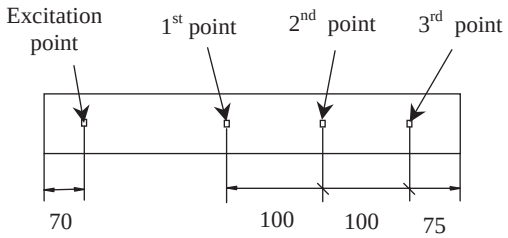

Fig. 14. Arrangement of measurement points and excitation point.

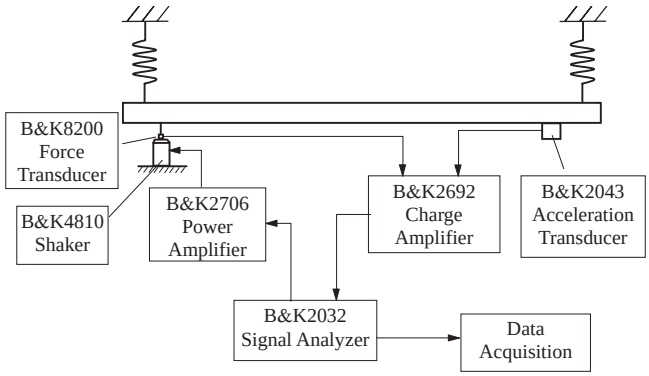

Fig. 15. A schematic of experiment set-up.

6 mm in diameter are drilled through the beam with their ends tapped for set screws, reducing the beam mass to 2.594 kg. The beam is suspended with four soft springs.

The beam is excited using a modal shaker with its location shown in Fig. 14. Three different locations on the beam are chosen for measuring the beam response as indicated in Fig. 14. The experimental set-up is illustrated in Fig. 15 with a description of measurement instruments used.

7.1. Test procedure

Our test procedure is as follows:

1. A broadband random excitation is applied to the beam with a maximum frequency of 6.4 kHz and an excitation force amplitude of 10 N. This would reveal the frequency characteristics of the beam. This test is performed separately on the solid beam (without damper holes), the drilled beam (without any particles), and the beam with different particle arrangements.
2. For each test arrangement, the half-power bandwidth method is applied to measure the damping ratio for a specified measurement point. Namely, $\zeta = \Delta\omega/2\omega_n$, similar to the approach taken in Refs. [7,9].
3. Tungsten carbide particles are used in the damping tests. Particles of three different sizes of $\phi = 0.1$, 0.3, and 0.5 mm are filled inside the holes in three different volumetric packing ratios of $\Theta = 50\%$, 90%, and 100%, respectively. Identical arrangements are made for all three holes. Density of the tungsten carbide material is 16 300 kg/m^3. At the full-packing ratio of 100%, the total particle mass is measured to be 432, 428, and 426 g for the three particle sizes, respectively, leading to a ratio of the particle mass to the solid beam mass of 14.77%, 14.63%, and 14.56%, respectively.

7.2. Modal characteristics of the beam

The first set of tests is to determine the modal characteristics of the original solid beam and the drilled beam but with empty holes. The frequency responses of the beams under the broadband random excitation are shown in Fig. 16(a) as measured at the first measurement point. While the original solid beam has natural frequencies ω_n at 331.6, 914.1, 1792.0, 2962.3, 4425.2, and 6180.7 Hz for the first six modes, the empty longitudinal holes make relatively small changes in the first five modes. The amplitudes at the resonance frequencies decrease with the drilled holes, on an average of 3.5%.

It is noticed that the test of the drilled beam shows an additional natural frequency at 5100 Hz which is absent from the original solid beam. A direct analysis using the Bernoulli–Euler beam theory shows that no such mode exists for bending motion. Therefore, we have performed a FEM analysis of the drilled beam, which predicts a *torsional* mode at 5074 Hz. Its modal shape of FEM analysis is shown in Fig. 16(b). Apparently, this modal shape in torsion got excited in the test of the drilled beam, but it was not at the first test of the solid beam. This peculiar situation was examined in Ref. [27].

Next, another set of tests is conducted for various combinations of particle size and volumetric packing ratio. Fig. 17 shows the effect of the added particles in attenuating the frequency response over the range of the first six modes for a case of 0.5 mm particles with $\Theta = 100\%$ at the first

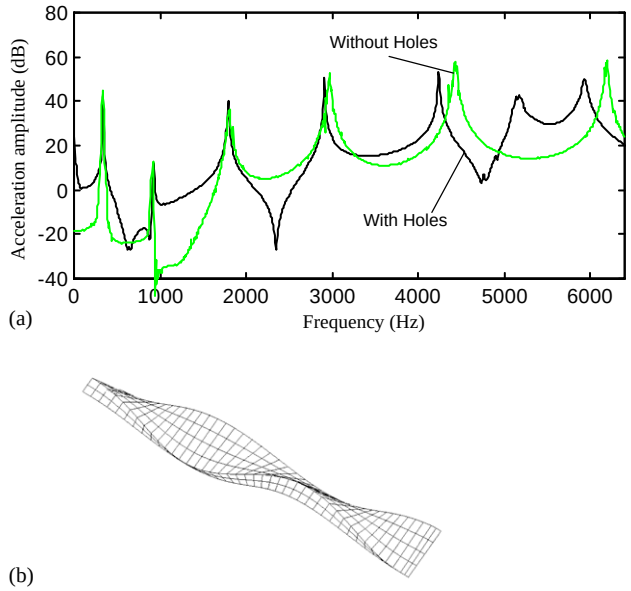

Fig. 16. (a) Acceleration amplitude (dB) of the beam with and without the damper holes. (b) A torsional mode of the beam at 5074 Hz.

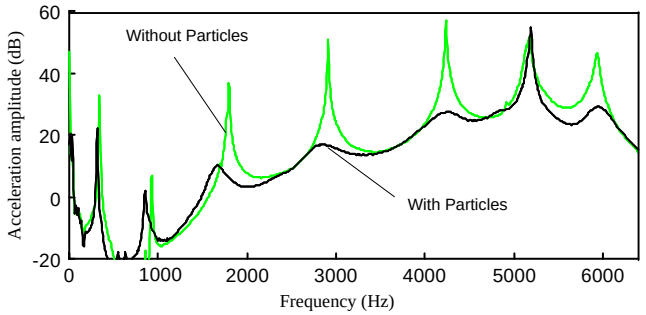

Fig. 17. Acceleration amplitude (dB) of the drilled beam with and without the particles.

Table 3
Damping ratio of the beam

	Mode				
	1st	2nd	3rd	4th	5th
Without particles	0.00298	0.00250	0.000571	0.00112	0.00113
With particles	0.0128	0.00402	0.0649	0.0354	0.101

measurement point. The damping ratio at each resonance is summarized in Table 3. From the table and Fig. 17, we observed that the damping performance of the particles is remarkable and extremely high. The level of damping even reaches $\zeta \approx 10\%$ for the fifth mode. Such a strong

damping effect has been consistently observed in particle dampers of other types of arrangements [2,6–14,22] as well. It is also typical in other cases of the parameter combination of our longitudinal damper discussed below.

It is further noticed that the added particles have virtually no effect on the torsional mode of the drilled beam of 5100 Hz for this particular case as shown in Fig. 17. Our physical and numerical models developed above are based on bending motion only, thus they cannot make any feasible prediction for this particular mode. Apparently, this mode is excited but the dampers are not effective. For other experimental tests (as discussed below), this torsional mode is also observed. The question about longitudinal particle dampers for suppression of torsional vibrations needs further study.

7.3. Comparison of numerical and experimental results

We have conducted a complete set of tests for each of the three particle sizes and each of the three volumetric packing ratios with a total of 27 combinations of the parameters. For each test case, the damping effect is also predicted with our numerical model. The numerical and experimental results of these cases are given in Table 4 in terms of the damping ratio at the first measurement point location.

Table 4
Damping ratio of model prediction and experiments

Particle diameter (mm)	Method	Θ (%)	Mode				
			1st	2nd	3rd	4th	5th
0.1	Experiment	50	0.00820	0.00133	0.00321	0.00228	0.0336
		90	0.00744	0.00302	0.00494	0.00540	0.0445
		100	0.00553	0.00151	0.00355	0.00358	0.0448
	Theory	50	0.0056	0.0035	0.0052	0.0049	0.034
		90	0.0069	0.0042	0.0074	0.0092	0.040
		100	0.0038	0.0040	0.0058	0.0073	0.0333
0.3	Experiment	50	0.0107	0.00234	0.0207	0.0167	0.0339
		90	0.0101	0.00241	0.0432	0.0288	0.0498
		100	0.00833	0.00291	0.039	0.0308	0.0622
	Theory	50	0.014	0.0031	0.018	0.0125	0.0285
		90	0.020	0.0068	0.036	0.0329	0.0371
		100	0.011	0.0072	0.027	0.0418	0.0528
0.5	Experiment	50	0.0101	0.00292	0.0247	0.0176	0.0458
		90	0.0118	0.00323	0.0486	0.0346	0.0984
		100	0.0128	0.00402	0.0649	0.0354	0.101
	Theory	50	0.0131	0.00351	0.0301	0.0169	0.0652
		90	0.0152	0.00483	0.0520	0.0231	0.0938
		100	0.0176	0.00629	0.0764	0.0364	0.0910

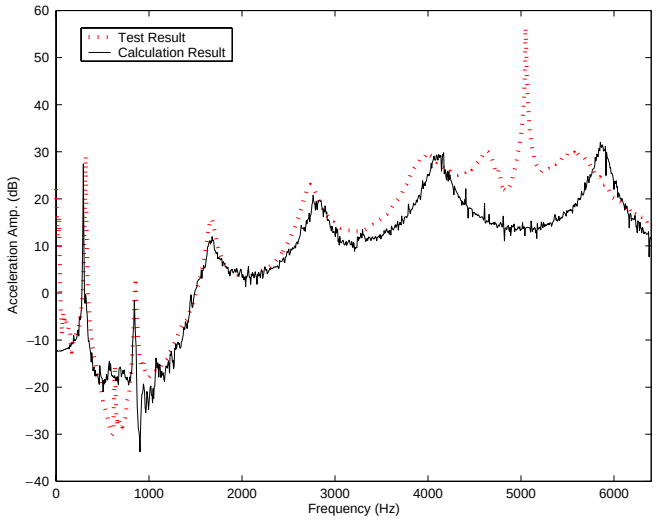

Fig. 18. Comparison between the test and the numerical results of frequency response for $\Phi = 0.1$ mm with a volumetric packing ratio of 100%.

Overall the numerical predictions agree with the experimental results very well. There are some specific observations worthy pointing out:

1. While the particle damping is significant for every mode of interest, it has a remarkably high effect for the fifth mode at 4425 Hz. The highest level of damping ratio reaches 10.1%, an increase of two orders of magnitude form that of the original beam. In our design of the experimental tests, simple guidelines were used and there were no optimization considerations. Clearly, the particular particle dampers are better suited for higher frequency range. Currently, we are pursuing a design methodology for optimization of particle damping.
2. Among the three particle sizes of 0.1, 0.3, and 0.5 mm in diameter, the relative errors between the model prediction and the experimental results are the least for the cases of 0.5 mm in size. It is also noticed that the damping ratio of model prediction tends to be higher than the experimental observation. Precise reasons for these features of the prediction error are yet understood, although we may speculate that our model of impacting spheres may overestimate the actual amount of particles participating in impacts with the beam while the vibration of the beam gets continuously attenuated over time. This is a rather complex situation and it needs further study, perhaps with a more sophisticated model such as the discrete element model on a particle–particle basis [15,16].

In Figs. 18–20, the frequency response over the entire range of the first six modes is shown with both the model prediction and the experimental data for the three particle sizes, respectively. The volumetric packing ratio is set at 100%. At the full-packing ratio, the major damping mechanism is the frictional shear between layers of the particles due to the longitudinal strain gradient as modelled in Section 4. There are seldom impacts of the particles on their containing holes. This is the favorable situation for our model and it shows in these figures that the model prediction agrees well with the experimental data. Again, in the experiments the torsional mode near 5100 Hz was excited, resulting in a sharp peak at the frequency and a higher response near the frequency in

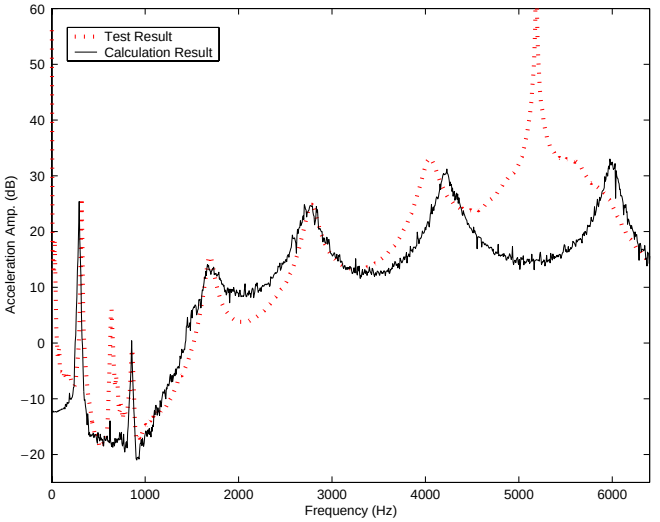

Fig. 19. Comparison between the test and the numerical results of frequency response for $\Phi = 0.3$ mm with a volumetric packing ratio of 100%.

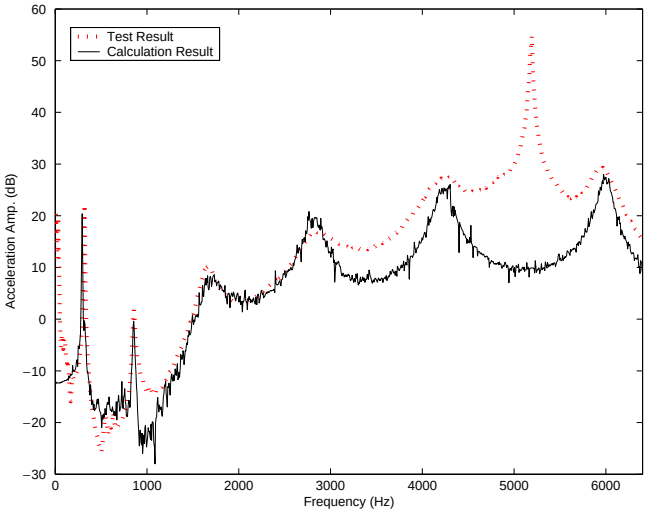

Fig. 20. Comparison between the test and the numerical results of frequency response for $\Phi = 0.5$ mm with a volumetric packing ratio of 100%.

Figs. 18–20. This is the primary reason for the difference between the numerical and experimental results shown in the figures.

8. Investigation of a plate

Another example for our numerical and experimental investigation is a plate structure. A steel plate specimen is sketched in Fig. 21(a) with dimensions of 300 mm in length, 300 mm in width,

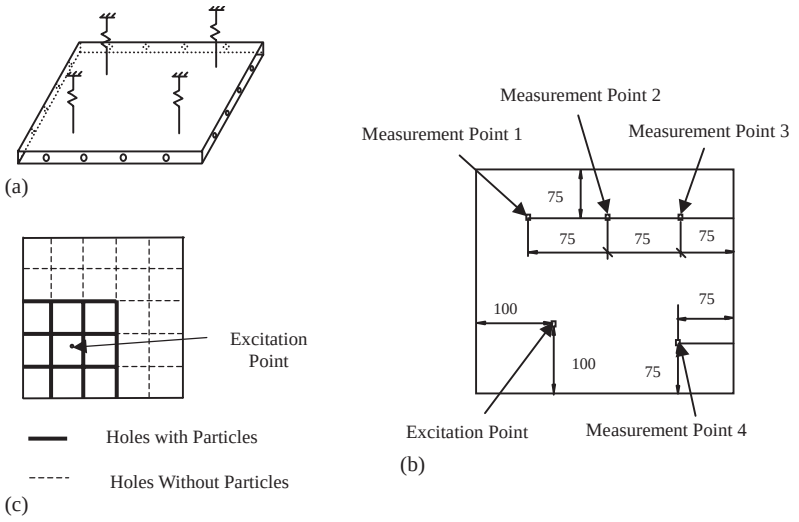

Fig. 21. (a) A schematic of the test plate, (b) locations of measurement and excitation points, and (c) partial filling of particles in the holes.

and 13 mm in thickness. The material is the same with the steel beam. Four holes of 6 mm in diameter are drilled and uniformly spaced in both the longitudinal and the latitudinal directions. The test plate is suspended with four soft springs. The locations of excitation and measurements are indicated in Fig. 21(b). The total volume of the eight holes counts for 5.8% of the volume of the plate. Thus, it is expected that these hole have a minor effect on the modal characteristics of the plate. A FEM analysis reveals the first eight natural frequencies of the drilled plate at 460.87, 677.36, 865.95, 1226.2, 2208.4, 2408.4, 2727.9, and 3716.3, respectively.

The particle holes are packed with the same tungsten carbide particles used for the beam tests with the particle size of $\phi = 0.5$ at full volumetric packing ratio of $\Theta = 100\%$. Two different patterns of particle filling are arranged. In the first arrangement, all holes are fully filled to their full length. The total particle mass is 671 g, which has a ratio of 7.6% to the mass of the drilled plate. In the second arrangement, a slightly over a quarter of the plate is treated with three holes in either direction filled in $\frac{3}{5}$ of their length as shown in Fig. 21(c). The total particle mass is 402 g, being 4.55% of the mass of the drilled plate. The treated portion of the plate contains the excitation point.

In Figs. 22 and 23 experimental results of frequency response in acceleration amplitude at the measurement locations #2 and #4 are shown over the entire range of the first eight modes for both cases of filling patterns. Responses at other two measurement locations are similar. We have two main observations from the experimental results. First, the damping performance of the particles is remarkably high especially in a high frequency range over 1500 Hz. For the lower resonance frequencies, the damping effect is not as high as usual. Second, the level of damping of the second arrangement of filling pattern is nearly as significant as in the first arrangement case. With the use of a little over half of the particles, nearly the same damping effect is achieved. It is noted that the particles holes of the second arrangement surround the excitation point. From a viewpoint of energy flow it seems that these particle dampers had a good chance to absorb the excitation energy. However, damper optimization is a subject of further study.

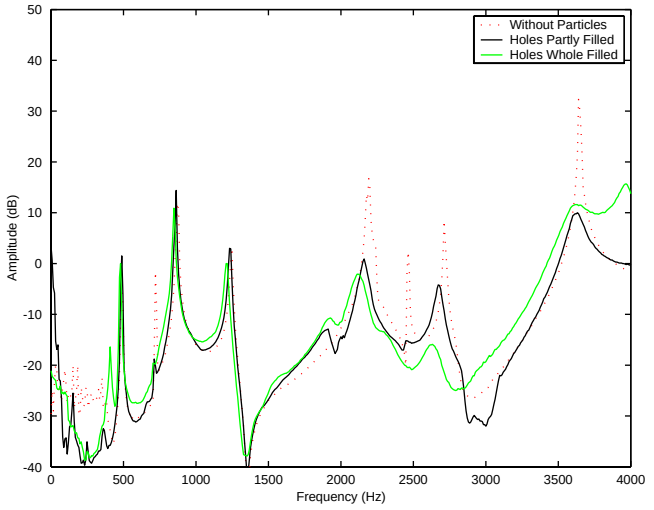

Fig. 22. Acceleration amplitude of the plate at measurement point #2 under different conditions of particle filling arrangements.

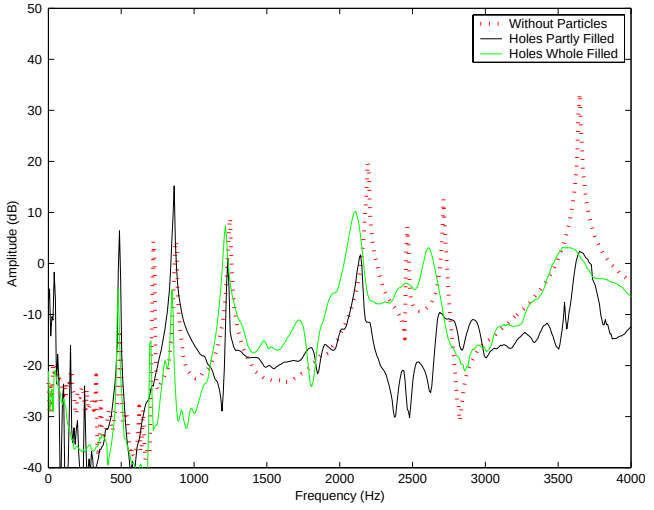

Fig. 23. Acceleration amplitude of the plate at measurement point #4 under different conditions of particle filling arrangements.

We also developed physical and numerical modelling techniques for the plate structure. The same shear friction and particle impact models also apply to the plate, while the standard plate bending equations are used in numerical calculation of structural response [26]. The iterative numerical solution procedure for the plate is essentially the same with that shown in Fig. 13. These numerical details shall be omitted here.

The results of model prediction and experimental testing at the measurement locations #2 and #4 are presented in Figs. 24 and 25 for the first damper arrangement and in Figs. 26 and 27 for the

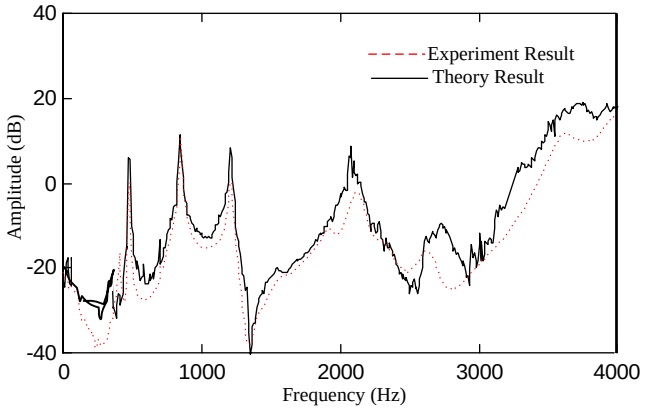

Fig. 24. Model prediction and experimental result of acceleration amplitude of the plate at measurement point #2 for the first damper arrangement.

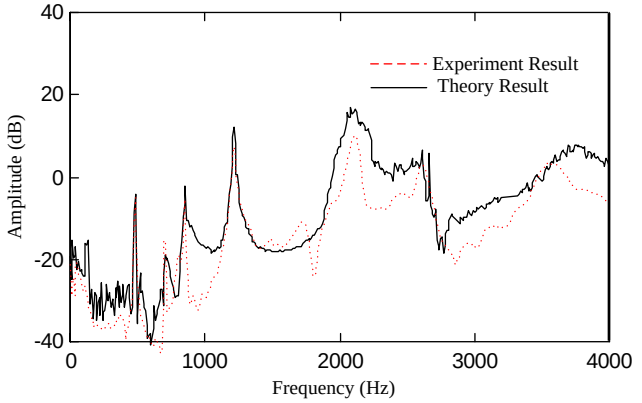

Fig. 25. Model prediction and experimental result of acceleration amplitude of the plate at measurement point #4 for the first damper arrangement.

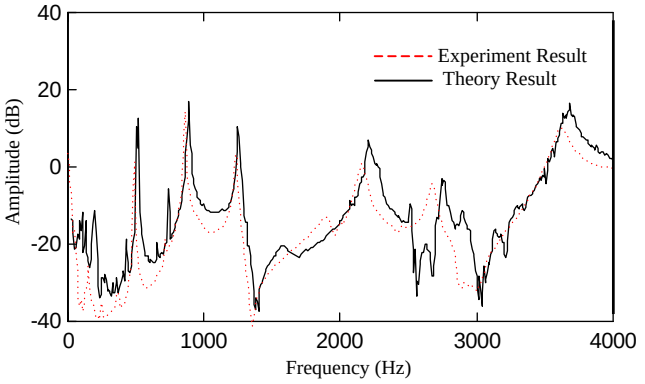

Fig. 26. Model prediction and experimental result of acceleration amplitude of the plate at measurement point #2 for the second damper arrangement.

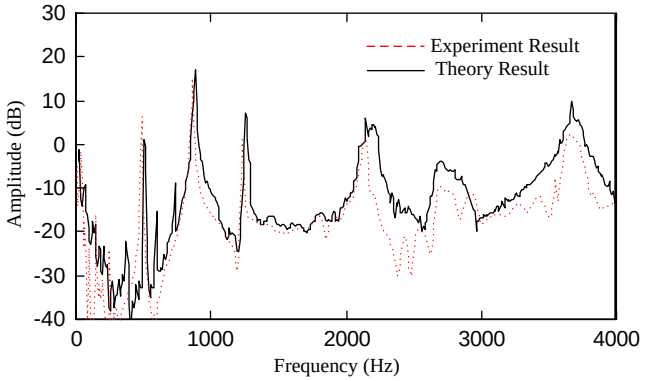

Fig. 27. Model prediction and experimental result of acceleration amplitude of the plate at measurement point #4 for the second damper arrangement.

second damper arrangement, all in acceleration amplitude. Overall, the model predictions agree very well with the experimental results. Within the frequency range up to 4000 Hz, their difference in acceleration amplitude is less than 10 dB.

More complete results of these experiments of beams and plates have been described in Ref. [27], where various transient behaviors of the vibrating systems under the particle damping treatments were further examined. Test results with a number of arrangements of the packed particles including different particle sizes and volumetric packing ratios are discussed there, showing that particle damping is highly non-linear while being remarkably effective within a broadband range [27].

9. Conclusions

The focus of this investigation is on a damping enhancement method with particulate materials. An elastic beam is treated with longitudinal holes embedded with metal particles. We have presented a physical model to take into account of the shear frictional forces between particle layers. Another model representing the impacts of the particles with the containing holes is also developed. Unlike traditional damping materials, the particle damping, in a form of friction and impact energy dissipation, is highly non-linear. A numerical procedure is presented in the paper for characterization of the damping effect. With these modelling tools, we performed numerical predictions for the beam structure with a number of arrangements of the packed particles including different particle sizes and volumetric packing ratios. The beam structure with the different damping treatments was experimentally tested. The experimental results validated the model predictions of the damping ratio of the damped beam. The numerical and experimental evaluations are also performed for an elastic plate with the particle damping treatment.

The particle damping is found to be remarkably effective. Although it is non-linear, a strong rate of energy dissipation is achieved within a broadband range. Moreover, the shear friction is determined to be the major contributing mechanism, especially at a high volumetric packing ratio near or at 100%. Our numerical and experimental findings should establish a significant role of shear frictional forces in utilization of the particle damping concept, especially when compared

with a transverse-type impact damper, such as a single-mass impact damper, where the damping mechanisms are dominated by the impact related phenomena [15,16,28]. Thus, the best damping effect might be achieved by using a design of different type of particle chambers involving an appropriate combination of impact, friction and shear mechanisms. Our current research is towards this direction.

Acknowledgements

The research work reported in this paper is sponsored in part by the Hong Kong Research Grants Council (Project No. CUHK4196/01E), a Croucher Chinese Visitorship of the Croucher Foundation of Hong Kong for Professor T.N. Chen, and the National Science Foundation of China (NSFC) under Grant No. 50390063.

References

[1] A.D. Nashif, D.I. Jones, J.P. Henderson, *Vibration Damping*, Wiley, New York, 1985.
[2] H.V. Panossian, Structural damping enhancement via non-obstructive particle damping technique, *American Society of Mechanical Engineers Journal of Vibration and Acoustics* 114 (1992) 101–105.
[3] H.V. Panossian, An overview of NOPD: a passive damping technique, *Shock and Vibration* 1 (6) (1991) 4–10.
[4] E.J. Richards, A. Lenzi, On the prediction of impact noise VII: the structural damping of machinery, *Journal of Sound and Vibration* 97 (4) (1984) 549–586.
[5] M. Abdel-Gawad, Passive vibration damping with non-cohesive granular materials, in: *Proceedings of Damping '91*, San Diego, CA, 1991, pp. 1–14.
[6] R.D. Friend, V.K. Kinra, Particle impact damping, *Journal of Sound and Vibration* 233 (1) (2000) 93–118.
[7] S.S. Simonian, Particle beam damper, in: *Proceedings of SPIE Conference on Passive Damping*, Vol. 2445, San Diego, CA, 1995, pp. 149–160.
[8] B.L. Fowler, E.M. Flint, S.E. Olson, Effectiveness and predictability of particle damping, in: *Proceedings of SPIE Conference on Damping and Isolation*, Newport Beach, CA, March 2000.
[9] J.J. Hollkamp, R.W. Gordan, Experiments with particle damping, Passive damping and isolation, in: *Proceedings of SPIE*, Vol. 3327, San Diego, CA, March 1998, pp. 2–12.
[10] S. Ekwaro-Osire, I.C. Desen, Experimental study on an impact vibration absorber, *Journal of Vibration and Control* 7 (2001) 475–493.
[11] C.N. Bapat, S. Sankar, Single unit impact damper in free and forced vibration, *Journal of Sound and Vibration* 99 (1985) 85–94.
[12] N. Popplewell, S.E. Semergicil, Performance of bean bag impact damper for a sinusoidal external force, *Journal of Sound and Vibration* 133 (2) (1989) 193–223.
[13] A. Papalou, S.F. Masri, An experimental investigation of particle damper under harmonic excitation, *Journal of Vibration and Control* 4 (1998) 361–379.
[14] C. Saluena, T. Poschel, S.E. Esipov, Dissipative properties of vibrated granular materials, *Physics Review* E59 (4) (1999) 4422–4425.
[15] T. Chen, K. Mao, X. Huang, M.Y. Wang, Dissipation mechanisms of non-obstructive particle damping using discrete element method, in: *Proceedings of SPIE International Symposium on Smart Structures and Materials*, Vol. 4331, Damping and Isolation, Newport Beach, CA, March 2001, pp. 294–301.
[16] K.M. Mao, Z.W. Xu, M.Y. Wang, T.N. Chen, Efficient computation of particle motions in discrete element modelling of particle damping, *Eighth International Symposium on Plasticity and Impact Mechanics*, New Delhi, India, March 2003, pp. 994–1005.
[17] P. Cundall, O. Strack, A distinct element model for granular assemblies, *Geotechnique* 29 (1979) 47–65.

[18] D.E. Wolf, Modelling and computer simulation of granular media, in: K.H. Hoffmann, M. Schreiber (Eds.), *Computational Physics: Selected Methods—Simple Exercises—Serious Applications*, Springer, Heidelberg, 1996.
[19] P.W. Cleary, DEM simulation of industrial particle flows: case studies of dragline excavators, mixing in tumblers and centrifugal mills, *Powder Technology* 109 (2000) 83–104.
[20] B.K. Mishra, C.V.R. Murty, On the determination of contact parameters for realistic DEM simulations of ball mills, *Powder Technology* 115 (2001) 290–297.
[21] M.E. Fayed, L. Otten (Eds.), *Handbook of Powder Science and Technology*, 2nd Edition, Chapman & Hall, New York, 1997.
[22] R. Sommer, Sports equipment for ball games having an improved attenuation of oscillations and kick-back pulses and an increased striking force, US Patent 5454562, October 1995.
[23] R. Dobry, T.-T. Ng, Discrete modelling of stress–strain behavior of granular media at small and large strains, *Engineering Computation* 9 (1992) 129–143.
[24] K.L. Johnson, *Contact Mechanics*, Cambridge University Press, Cambridge, UK, 1985.
[25] L. Vu-Quoc, X. Zhang, O.R. Walton, A 3-D discrete-element method for dry granular flows of ellipsoidal particles, *Computer Methods in Applied Mechanics and Engineering* 187 (2000) 483–528.
[26] S.G. Kelly, *Fundamentals of Mechanical Vibrations*, 2nd Edition, McGraw-Hill, New York, 2000.
[27] Z.W. Xu, M.Y. Wang, T.N. Chen, An experimental study of particle damping for beams and plates, *American Society of Mechanical Engineers, Journal of Vibration and Acoustics* 126 (2004) 141–148.
[28] K.M. Mao, M.Y. Wang, Z.W. Xu, T.N. Chen, Simulation and characterization of particle damping in transient vibrations, *American Society of Mechanical Engineers, Journal of Vibration and Acoustics* 126 (2004) 202–211.